11th International Conference on Fracture Mechanics of Concrete and Concrete Structures
FraMCoS-11
J. M. Chandra Kishen, A. Ramaswamy, S. Ray and R. Vidyasagar (Eds)
https://doi.org/10.21012/FC11.092322

FRACTURE PROPERTIES OF CONCRETE IN COMPRESSION – DETERMINATION OF A "COMPRESSIVE FRACTURE ENERGY" USING DIGITAL IMAGE CORRELATION TECHNIQUE

N. MUELLER[*], A. GOLDACK[*] AND S. ANDERS[†]

[*] University of Wuppertal
Institute of Structural Engineering – Chair of Statics and Dynamics of Structures
Pauluskirchstraße 7, 42285 Wuppertal, Germany
e-mail: goldack@uni-wuppertal.de, www.statik.uni-wuppertal.de

[†] University of Wuppertal
Institute of Structural Engineering – Chair of Construction Materials
Pauluskirchstraße 11, 42285 Wuppertal, Germany
e-mail: s.anders@uni-wuppertal.de, www.baustoff.uni-wuppertal.de

Key words: Compressive Fracture Energy, Compressive Concrete Failure, Digital Image Correlation (DIC), Strain-Softening, Inelastic Energy, Localization

Abstract: The fracture process and damage of concrete in compression is a highly non-localized phenomenon, because numerous micro-cracks occur throughout the entire specimen during loading. In contrast, tensile or flexural failure is characterized by a single macro-crack, for which a conventional "fracture energy" can be provided. For concrete in compression, the situation is more complex, because the type of failure may differ between "crushing", "splitting" and "spalling". However, a compressive fracture energy is needed for nonlinear FE calculations e.g. for many numerical degradation models of concrete. Its experimental determination and reliable values are still very scarce. This paper presents the results of several tests performed at the University of Wuppertal on concrete specimens with a height to diameter ratio of 4 to determine the compressive fracture energy of these specimens. The authors used acrylic rods with strain gauges attached and compared the results with measurements using Digital Image Correlation technique (DIC). Compared to the acrylic rods with strain gauges, the DIC system is very robust and more reliable data can be collected. The paper shows new and flexible possibilities offered by DIC to evaluate the compressive fracture energy and to identify the crushed volume without the limitations of conventional measuring methods. So far, DIC systems have not been systematically used to determine compressive fracture energies of concrete. The authors present a method to evaluate compression tests using a DIC system. The compressive fracture energy is determined in a varying number of sections over the entire specimen height. It can be shown that the calculated compressive fracture energy clearly depends on the chosen number of sections. It is demonstrated, that the DIC technology can overcome the inherent problem of conventional measuring techniques, which enforce a predefined partitioning of the specimens. With DIC technology, partitioning can be adjusted during post-processing. However, further tests are needed to show whether this method can be used to determine reliable values for the compressive fracture energy.

1 INTRODUCTION

In tensile or flexural failure, the "fracture energy" is both, a recognized material property as well as an established concept in material models. For the determination of the fracture energy in tension, often denoted as G_f, several instructions exist [2, 3]. Additionally, in [1] and [4] estimations for the fracture energy exist, partially including effects such the maximum grain size. Seen from the modelling as well as experimental it is advantageous, that tensile failure of concrete is a localized phenomenon, usually reducing to a single crack. In contrast, the fracture process of concrete in compression is highly non-localized, because numerous micro-cracks occur throughout the specimen during loading. The fracture process and characteristics in compression are comprehensively described in [5] starting from the meso-scale failure mechanism up to stress-strain diagrams including strain-softening. Additionally, requirements for specific tests are outlined, which are later summarized and published in [6]. In compression, the type of failure can differ between "crushing", "splitting" and "spalling". However, a kind of "compressive fracture energy" is needed for many numerical degradation models of concrete and for nonlinear Finite Element calculations, but its experimental determination is still very scarce.

Different approaches for the determination of a "compressive fracture energy" are compared and discussed in this contribution. The Digital Image Correlation technique seems to be a promising approach to characterize the type of compressive failure and quantify the energy consumed in the fracture process.

2 STATE OF THE ART

2.1 Phenomenon and application in numerical simulations

The compressive fracture energy is successfully used to describe the inelastic deformations and strains of cracked concrete. It is particularly used in numerical simulations with nonlinear FE methods as input parameter of various constitutive models, such as the Coupled Plasticity Damage Model for concrete, see [7] and [8]. Furthermore, [9] and [10] use the fracture energy for compressive failure to describe the fatigue behavior of concrete in compression.

Various authors have shown that failure of a concrete specimen in compression localizes in a specific volume if the specimen is sufficiently slender. [10] and [11] found that the inelastic deformation and crushing energy of specific volume is independent of slenderness when the slenderness is given in terms of e.g. height to diameter is greater than 2. See also Figure 1.

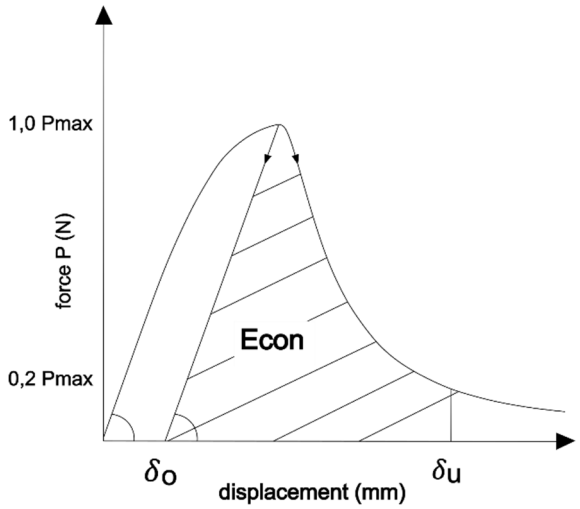

Figure 1: Definition of compressive fracture energy dissipated in the fracture process zone in a load displacement diagram, according to [12].

The compressive fracture energy as localized phenomenon is based on the fracture volume V_p with a fracture length L_p and the cross-sectional area of the specimen. In particular, a volumetric failure rather than a specific cross section failure has been observed for compressive failure by [11], [12], [13] and [14]. Note, that the fracture length must be smaller than the length of the specimen.

The question is, whether this localized compressive fracture energy is a material property such as Young's modulus, strength or plastic strain. Although the compressive fracture energy is very important for numerical simulations of structural concrete components and reinforced concrete structures, only few

data is available. E.g. [1] and [4] provide no values for simulation or experimental test-setups.

2.1 Definition of the compressive fracture energy

In this paper, the compressive fracture energy g_{cl} is defined as the energy dissipated in the fracture process zone as shown in Figure 2 and Equation (1) based on work of [10],

$$g_{cl} = \frac{E_{con}}{A_c\, L_p}$$

$$g_{cl} = \frac{\int_0^{\delta_u} P(\delta)d\delta - \int_0^{\delta_0} P(\delta)d\delta}{A_c\, L_p}$$

$$g_{cl} = \frac{\int_0^{\delta_u} P(\delta)d\delta - W_p}{A_c\, L_p}\ [\frac{Nmm}{mm^3}] \qquad (1)$$

with the energy E_{con}, which is consumed in the failure zone of the specimen, the cross section A_c of the specimen, the length L_p of the fracture process zone, the load $P(\delta)$ on the specimen, the overall displacement δ and the plastic work W_p.

This definition of the compressive fracture energy includes all possible failure modes like crushing and shear failure, as is the case, for example, in the compression damage zone model by [15]. This model uses inelastic strains and a displacement w (in direction of the load) caused by a shear crack in diagonal shear plane.

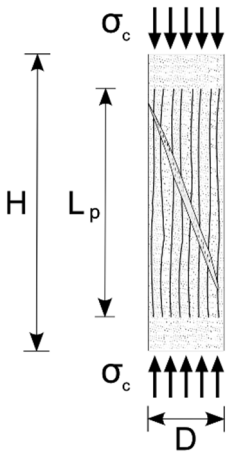

Figure 2: Compressive damage zone with shear crack according to [15].

The determination of the compressive fracture energy is laborious. This is due to the different crack patterns and failure modes that can occur in the specimens. Furthermore, experiments usually must be performed in deformation control mode to avoid brittle failure. Care must also be taken regarding the loading platens, because conventional steel platens, brushes or use of Teflon foils delivers different results for post-peak deformations [2]. Another important factor is the effect of slenderness. In [2], slenderness in terms of height (H) to diameter (D) was varied from 0.5 to 2.0. Experiments by e.g. [11], [12] or [16] show that the softening branch gets more brittle with an increasing slenderness, at least as long as strain is calculated using the total length L of a specimen (see also Figure 3).

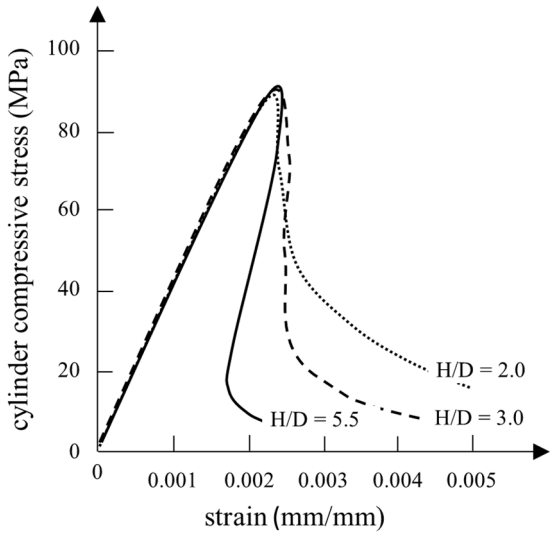

Figure 3: Increasing brittleness of strain softening behavior with increasing slenderness of the specimen simplified after [16].

The increasing brittleness is attributed to the fact, that compressive failure is a localized phenomenon. As slenderness increases, energy is dissipated in only a portion of the specimen, while the remaining portions are elastically relieved and further deteriorate the already damaged portion of the concrete.

2.2 Failure zone, facture length and stress-strain relation

The specimen, especially a slender specimen, has different areas where different stress-strain relations can be found due to localization of failure. Since fracture does not

occur along the entire length of slender specimens, Equation (1) applies only to the compressive fracture zone. According to Figure 4 by [14], the fracture process zone shows large strains and a flat curve in the post-peak regime of the stress-strain diagram. Other parts of the specimen are elastically relieved with decreasing test load, called the unloading zone, or have a mixture of both, called transition zones. In the unloading zone, only plastic deformation can remain.

The resulting stress-strain diagram for the entire specimen is the sum of all stress-strain relations in the different zones as shown in Figure 4. If a small fracture process zone and a large unloading zone appear, the resulting stress-strain curve is very steep in the post-peak regime. There could even be a snap-back behavior (see Figure 1 and Figure 3c).

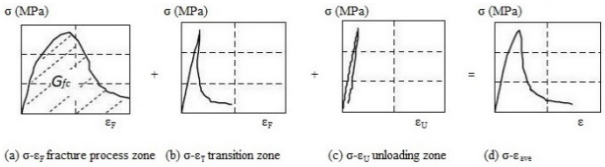

Figure 4: Resulting stress-strain curve by stress-strain relation of compressive fracture zone, transition zone and unloading zone according to [14].

The fracture length L_p is not estimated by observing the crack pattern on the specimen. It is determined based on the stress-strain diagrams of the fracture process zone. Only those stress-strain curves that show a clear fracture process zone are evaluated for the compressive fracture energy and only those sections count towards the fracture length.

The fracture length L_p of the compressive fracture zone as given in literature has broad scatter. [12] found Equation (2) using the compressive strength f_c' to fit the test data with a crushing failure.

$$L_p = \frac{1300}{\sqrt{f_c'}}\ [mm] \tag{2}$$

With a compressive strength of $f_c' = 20\ MPa$ the fracture length is 290 mm, which is about 2.9 times the diameter. [16] mentioned fracture lengths for normal- and high strength concrete being about twice the diameter.

3 EXPERIMENTAL DETERMINATION OF THE COMPRESSIVE FRACTURE ENERGY

3.1 Tests with acrylic rods

[12] as well as [14] describe the determination of a compressive fracture energy. In contrast to measurements by e.g. [16] or [10], who only measured the total deformation, they included a concept for local strain measurements throughout the whole length of the specimens. They performed tests, in which acrylic rods were placed in the center of specimens. The rods cover the full height of the specimen and are embedded during concreting. The acrylic rods were notched at 40 mm intervals and strain gauges were applied on each interval. The cylindrical specimens of 100 mm and 150 mm diameter D had H/D ratios of 1, 2, 3, 4, 5 and 6, where H is the height of the specimen. The maximum aggregate size was 40 mm. In particular, a volumetric failure by crushing rather than a specific cross-section failure as in tensile fracture was observed.

At the University of Wuppertal in the lab of the Institute of Structural Engineering the aforementioned methodology was applied to study the compressive fracture energy of concrete. The specimens in this study had a diameter of 100 mm and a height H to diameter D ratios of H/D = 2, 4, 6. The tests were performed in an universal electro-mechanical 250 kN testing machine. Teflon pads were used between the edges of specimens.

To ensure crushing failure and a distinct ductility in the strain softening regime, a concrete with mean compressive strength of about 10 MPa at the time of testing was used. The maximum grain size equaled 8 mm and the volume of about 675 liter per m³.

Furthermore, acrylic rods with a cross section of 10 mm x 10 mm were casted in the specimens. The rod was notched at regular intervals and divided into sections of 52 mm as shown in Figure 5.

In each section, two electrical strain gauges with lengths of the measuring grid of 6 mm (type: HBK 6/120 LY41A) were glued opposite each other and then wired. The wires could be

led inside the acrylic bar to the end and from there outside the formwork.

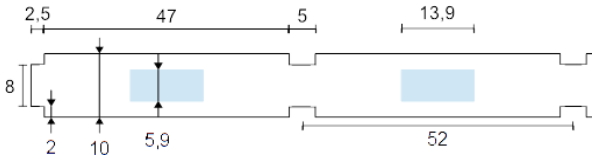

Figure 5: Principal layout of an acrylic rod in (mm) with strain gauges (type HBK 6/120 LY41A, measuring grid length 6 mm) for strain measurement.

This method allowed measuring the strains section by section. However, the accompanying stresses were calculated using the load cell of the testing machine and the cross-section of the specimen. The stiffness of the cross-section of the acrylic bar, at $EA = 300\ kN$, is much lower than that of the undamaged concrete cross-section at about $EA = 60000\ kN$. However, it was not possible to estimate the extent to which the rod influences the cracking behavior of the specimen and thus also the result. Figure 6 exemplarily shows a H/D = 2 specimen where the acrylic rod seems to be buckled.

Figure 6: Acrylic rod buckling within a H/D = 2 specimen (Photo: N. Heider).

Major disadvantages of this methodology are the big efforts for preparing the rod, difficult concreting conditions and possibly the loss of strain gauges. Figure 7 shows an instrumented rod for a H/D = 6 specimen. Furthermore, there is no investigation about the adequate length of the sections. The length of 52 mm of each section was chosen randomly.

The load was applied in deformation control. In particular, several loops with unloading and reloading were run in the post-peak regime to quantify the damage of the concrete. The load loops also helped to detect if strain gauges failed.

Figure 8 and Figure 9 show the result of the study for a selected sample with H/D = 4. The sample Z4_3 in Figure 8 on the left showed a crushing failure that is located within the lower third of the specimen. It should be noted, that the failure was not initiated at the end of the specimen caused by spalling or a diagonal shear crack. The diagrams at the right show the stress strain relations of each section. The specimen was divided into 8 sections for strain measurements.

Figure 7: Acrylic rod with 24 strain gauges for the H/D = 6 specimen (Photo: N. Heider).

Figure 9 shows comparable results for the specimen Z4_1 with H/D = 4 and a diagonal shear crack. The failure zone is located in sections 2, 3, 4, 5, 6, which exhibit large strains in the post-peak range. The other sections show unloading with plastic deformation or behave like a transition zone. The fracture length results in total from 5 sections, which is in this case $L_p = 250\ mm$.

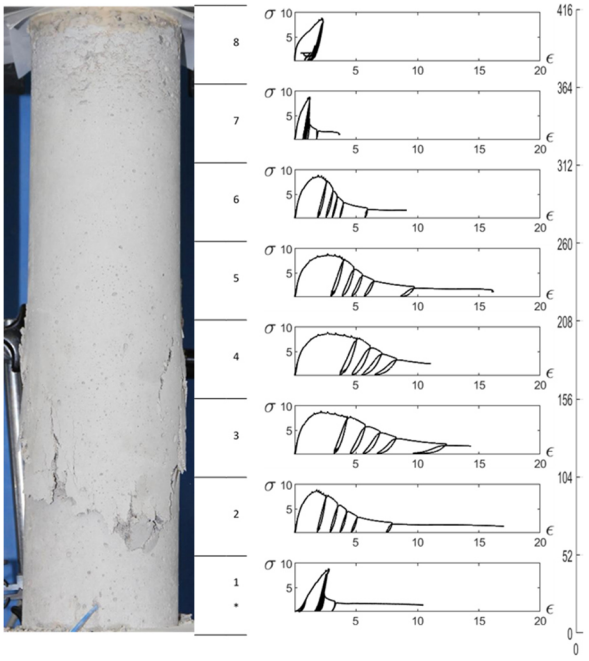

Figure 8: H/D = 4 specimen Z4_3 with section wise stress-strain diagram (stress in (MPa), strain in (mm/m)) (Photo: N. Heider).

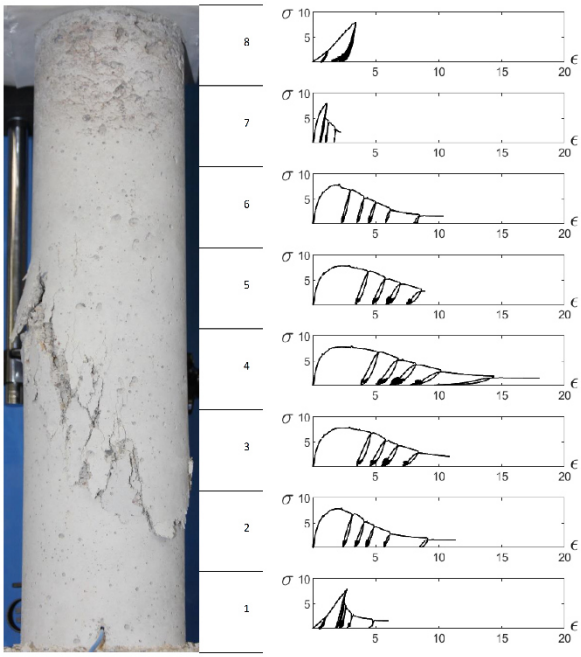

Figure 9: H/D = 4 specimen Z4_1 with section wise stress-strain diagram (stress in (MPa), strain in (mm/m)) (Photo: N. Heider).

The results of this study at the University of Wuppertal with the acrylic rods show:

- For slender specimens, failure in compression occurs in a localized fracture process zone, which is only a sub-region of the specimen. This could be observed for specimens with H/D = 4 and more. The length of the fracture process zone was approx. 2.5 times the diameter D.

- The stress-strain curves in several sections clearly show large strains of 5 mm/m and more. The curves show a very flat shape

- In unloading zones, stress-strain curves show an elastic relief with residual plastic strains, especially for the specimen Z4_1 in upper section 8 in Figure 9. The results of this study clearly confirm the findings of [12] as well as [14].

It should be noted that the stress-strain curves of the fracture process zone in Figure 8 and Figure 9 have different slopes and end at different strains. The residual stiffness as given by the last unloading-reloading path of Z4_1 in section 4 is much flatter than that in section 2, displaying greater damage. The stress-strain curves for both sections 1 do not show a clear unloading behavior. In addition, the last unloading-reloading path, which is included in section 4, is missing from the stress-strain curve in sections 3 and 5. Perhaps the strain gauges were damaged.

3.2 Tests with Digital Image Correlation System (DIC)

Encouraged by the results obtained with the acrylic bars and to overcome their shortcomings, the Institute of Structural Engineering has purchased a 3D Digital Image Correlation (DIC) system by LaVision equipped with 4 cameras to observe two surfaces independently.

DIC is a non-contact optical technique for tracking the movement of naturally occurring or applied surface patterns. The surface pattern can be applied with spray paint. To achieve a good contrast, it is recommended to use, for example, a black lacquer on a white primer.

A possible experimental setup is shown in Figure 10. The images are taken by digital cameras during the experiment and recorded directly on the computer. Lights are used to increase contrast within the surface pattern. Once the images have been captured, the image series is processed on the computer using DIC software. During the processing the pattern is divided into individual subsets, which are

compared between successive images. Algorithms are used to analyze the intensity distributions of these subsets in order to determine the local displacement vectors and strain fields.

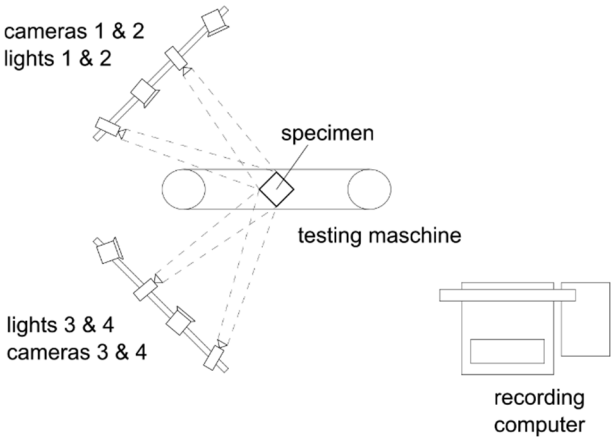

Figure 10: Sketch of the test-setup with DIC system for measuring two surfaces simultaneously.

After processing with DIC software, digital strain gauges and extensometers can be used to plot strain over time. These virtual strain gauges may have almost any length and orientation and can be positioned anywhere on the specimens. With the force signal of the testing machine, it is also possible to generate stress-strain curves.

The DIC system therefore overcomes the disadvantage of strain gauges and notched rods, as described in the previous section, which have predefined and fixed positions and measuring lengths. Furthermore, the formation of cracks cannot lead to a loss of strain gauges. The virtual strain gauges can be adjusted based on the crack pattern in the post-processing. In addition, the software has a programming interface to automatize the evaluation of the data in the near future, including identification of the fracture process zone.

Figure 11 shows the test set-up with the DIC System in the lab. A typical problem is the space on and around the testing machine for the cameras as well as the lightning. Furthermore, LVDTs were used in addition for plausibility checks, which restrict the free view of the test specimen.

Figure 11: Test-setup with DIC system (Photo: C. Wegert).

In this series of experiments, prismatic samples with an edge length a of 100 mm by 100 mm and a height H of 400 mm were tested in order to investigate the possibilities of a DIC system in determining the compressive fracture energy of concrete specimens. The samples were preferred over the cylinders, because the flat surfaces can be evaluated more precisely.

To ensure crushing failure, the concrete mixture was optimized regarding the maximum grain size and percentage of aggregates. In this campaign, 690 liters of 32 mm river gravel were used as maximum grain size. The compressive strength at time of testing equaled about 22 MPa tested using cubes with a side length of 150 mm.

The specimen PK 1 was measured with the DIC system and evaluated by virtual strain gauges in the software with different length. Figure 12 shows the stress-strain curves for 8 sections with virtual strain gauges of approx. 50 mm length and Figure 13 the stress-strain curve when only 4 strain gauges with a length of 100 mm were calculated. In both cases, the virtual strain gauge was placed in the middle of the surface. The breaking load of the specimen is 157.7 kN and the corresponding to a compressive strength of about 16 MPa.

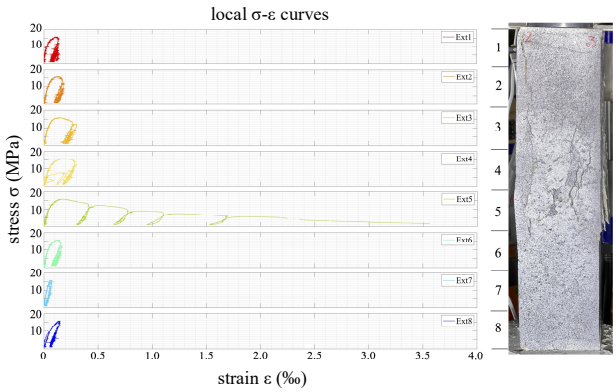

Figure 12: Specimen PK 1 with H/a = 4 with eight evenly distributed strain gauges (n = 8) (stress in (MPa), strain in (mm/m)) (Photo: C. Wegert).

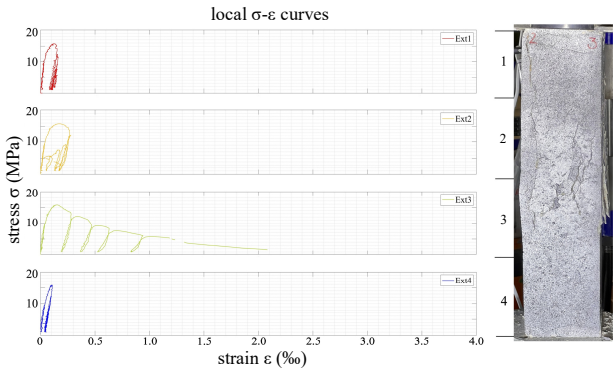

Figure 13: Specimen PK 1 with H/a = 4 with four evenly distributed strain gauges (n = 4) (stress in (MPa), strain in (mm/m)) (Photo: C. Wegert).

The evaluation with 8 virtual strain gauges (n = 8) in Figure 12 shows a distinct fracture process zone only in section 5. The length of the virtual strain gauge in this case is 50 mm only. In this section, only 60% of the entire compressive fracture energy is consumed. All other sections have less than 15% of the overall energy consumption, which is 0.0119 Nmm/mm³. According to [12], they do not contribute to the fracture length. On the other hand, the fracture process zone should comprise at least 85% of the entire energy consumption according to [12].

In contrast, the length of the strain gauge in the n = 4 evaluation is twice as long, 100 mm. Comparing the stress-strain curves in the fracture process zone in section 3, it can be seen that the post-peak region is much steeper and the strain achieved at the end is only 2.5 mm/m compared to 3.5 mm/m with n = 8. This could indicate that in the evaluation with n = 4 in section 3 the transition zone and the unloading zone have a significant influence.

The length of the virtual strain gauges as well as the cross-sectional area define the volume in which the calculated compressive fracture energy is consumed. The evaluation with four virtual strain gauges (n = 4) indicates a bigger volume of the fracture process zone per section than the evaluation with 8 virtual strain gauges (n = 8). Consequently, the compressive fracture energy according to Equation (1) is much smaller. In both evaluations, the transition region plays a role, since not only plastic work is performed here, but fracture begins and then, however, the curve changes to a linear elastic unloading.

Figure 14 shows the compressive fracture energy g_{fc} section wise for n = 4, 7, 8 sections. The compressive fracture energy $g_{fc}(5,8) = 0.0475 \frac{Nmm}{mm^3}$ in section 5 for n = 8 is the highest value. Compared to the highest value for n = 4 with $g_{fc}(3,4) = 0.0141 \frac{Nmm}{mm^3}$ it is 3.4 times higher. For n = 7 a peak value of $0.0404 \frac{Nmm}{mm^3}$ is calculated, which is about 85% of n = 8.

Even if the consumed energy is related to the cross-sectional area of the sample according to Equation (3), considerable variations in the results as shown in Figure 15 are found.

$$G_{cl} = \frac{E_{con}}{A_c} \left[\frac{Nmm}{mm^2}\right] \tag{3}$$

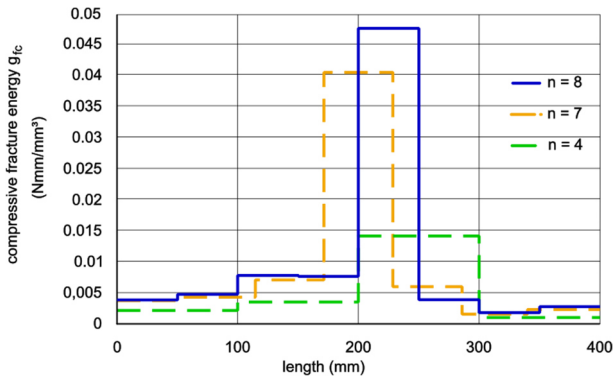

Figure 14: Compressive fracture energy g_{fc} (Nmm/mm³) section-wise for specimen PK 1 with H/a = 4 with different numbers of sections n.

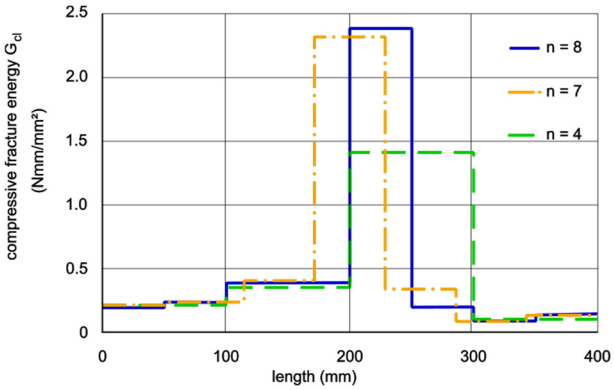

Figure 15: Compressive fracture energy per cross section $\boldsymbol{G_{cl}}$ (Nmm/mm²) section-wise for specimen PK 1 with H/a = 4 with different number of section n.

If the compressive fracture energy related to the cross section of the specimen is summed up over the entire sample length, for n = 8 a value of $G_{cl} = 3.98 \frac{Nmm}{mm^2}$, for n = 7 a value of $G_{cl} = 3.71 \frac{Nmm}{mm^2}$ and for n = 4 $G_{cl} = 2.06 \frac{Nmm}{mm^2}$ can be calculated. These results show considerable scattering of the fracture energy, which seems to depend on the length of the virtual strain gauges.

It must be noted, that all the results are neither compared nor checked with codes or recommendations regarding absolute values. All values given are only for comparison of the different effects using the DIC System. It has furthermore to be taken into account, that the post-processing discussed here only comprises one surface of each specimen. Parts of the mentioned scatter might also be attributed to uneven damage throughout the specimen.

Another question concerns the length L_p of the fracture process zone. For numerical calculations with the FE methods, the fracture length is an indispensable reference quantity in addition to the compressive fracture energy.

From Equation 2 according to [12], for cylinders, a maximum compressive stress of 16 MPa results in a fracture length $L_P = 328\ mm$. The test described in section 3.1 gave a L_p of approx. 250 mm. However, the experimental results presented in this paper using the DIC system show much shorter fracture lengths. Based on the definition of compressive fracture energy and the evaluation approach used in this paper, fracture length seems to depend on the number of virtual strain gauges. For n = 8 the fracture length seems to be only 50 mm increasing to 100 mm for n = 4.

Using the DIC system, however, it was still possible to evaluate samples at different points, even if the some parts of the surface have fallen off during the test. **Figure 16** shows specimen PK 5, where the fracture process zone can clearly be identified in the stress-strain relations over the entire length of the specimen, although the surface of the lower left corner is already missing. Again, the fracture process zone is clearly visible.

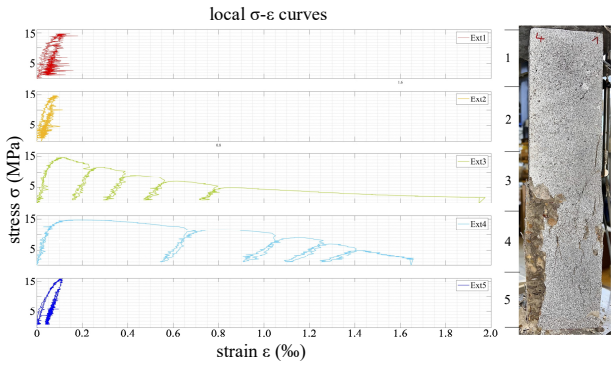

Figure 16: Specimen PK 5 with H/a = 4 (Photo: C. Wegert).

5 SUMMARY AND CONCLUSIONS

The experiments show that the DIC system provides comprehensive opportunities to further investigate compressive failure mechanisms of concrete and to quantify the compressive fracture energy. It is shown, that the method is very robust, since the arrangement of the strain gauges can be adjusted even if concrete is already spalling in the post-peak range. With the help of the DIC, the preparation of the samples and the evaluation of the experiments is much easier, although a suitable speckle-pattern must be applied for the measurements. Additionally, suitable lightning and well exposed images are challenging when using DIC.

Conventional measuring methods such as strain gauges or acrylic rods can only measure in pre-fixed sections. Thus, it cannot be assured that the measuring lengths suitably cover the fracture process zone. The DIC method offers

the possibility to adapt the positioning and size of sections for evaluation.

However, the application of the DIC system shows certain deviations compared to the tests with the acrylic rod. This concerns on the one hand the values for compressive fracture energy, but also the length of the failure zone. In addition, the measurements of the displacement field are limited to the surface of the sample.

The authors are currently working to further investigate the distribution of typical stress-strain curves on several surfaces of the same specimen, their relations and impact on the compressive fracture energy. Initial results with cylindrical specimens show that they could also be evaluated very well with the DIC system, despite the curved cross section.

With the results from the DIC system, the discussion about the concept of compressive fracture energy gets new possibilities and aspects. The DIC system is a very good tool for describing and understanding compressive failure as well as the problems involved in the definition and quantification of the compressive fracture energy. After all, a complex fracture process must be described comprehensively with a few parameters. Further tests must show whether this method can be used to determine reliable values for the fracture energy and estimate the length of the fracture process zone.

REFERENCES

[1] Comité Euro-International du Béton (CEB), 1993, CEB-FIB Model Code 1990. Thomas Telford Service Ltd., London, Lausanne.

[2] van Mier, J.G.M. (editor), 1997, Fracture processes of concrete – assessment of material parameters for fracture models. Taylor & Francis Group, CRC Press, Boca Raton, https://doi.org/10.1201/b22384.

[3] Rilem, 1994, RILEM Technical Recommendations for the testing and use of construction materials – FMC1 Determination of the fracture energy of mortar and concrete by means of three-point bend tests on notched beams. 1st edition, Tylor and Francis Group, CRC Press, https://doi.org/10.1201/9781482271362.

[4] Fédération International du Béton (fib), 2013, fib Model Code for Concrete Structures 2010. Wilhelm Ernst & Sohn Verlag, Berlin.

[5] van Mier, J.G.M., 1998. Failure of Concrete under uniaxial compression: An overview. Proceedings of FRAMCOS-3 Gifu (Japan), Aedificio Publishers, Freiburg, Germany

[6] Shah, S.P., van Mier, J.G.M., Banthia, N., Bascoul, A., Berthaud, Y., Bittnar, Z., Buyukozturk, O., Carpinteri, A., Elices, M., Ferrara, G., Gettu, R., Gylltoft, K., Hassanzadeh, M., Hawkins, N., Horii, H., Karihaloo, B.L., König, G., Kotsovos, M., Labuz, J., Markeset, G., Reinhardt, H.W., Schorn, H., Stang, H., Thienel, K.-Ch., Ulfkjær, J.-P., 2000. Test method for measurement of the strain-softening behaviour of concrete und uniaxial compression. Materials and Structures, Vol. 33, July 2000, pp. 347-351

[7] Alfarah, B., López-Almansa, F., Oller, S., 2017. New methodology for calculating damage variables evolution in Plastic Damage Model for RC structures. Engineering Structures 132:70–86. DOI: 10.1016/j.engstruct.2016.11.022.

[8] Krätzig, W. B., Pölling, R., 2004. An elasto-plastic damage model for reinforced concrete with minimum number of material parameters. Computers & Structures 82 (15-16):1201–1215. DOI: 10.1016/j.compstruc.2004.03.002.

[9] Pfister, T., Pfanner, D., Stangenberg, F., Petryna, Y.S., 2003, Modeling of concrete response under fatigue. Computational Modelling of Concrete Structures, Proceedings of the Euro-C Conference 2003, St. Johann im Pongau.

[10] Mu, B., Subramaniam, K.V., Shah, S.P., 2004. Failure Mechanism of Concrete under Fatigue Compressive Load. In: Journal of Materials in Civil Engineering 16 (6): 566–572. DOI: 10.1061/(ASCE)0899-1561(2004)16:6(566).

[11] Jansen, D.C., Shah, S.P.,1997. Effect of Length on Compressive Strain Softening of

Concrete. Journal of Engineering Mechanics 123 (1):25–35. DOI: 10.1061/(ASCE)0733-9399(1997)123:1(25).

[12] Nakamura, H., Higai,T., 2001, Compressive fracture energy and fracture zone length of concrete. Modeling of inelastic behavior of RC structures under seismic loads.

[13] Lertsrisakulrat, T., Watanabe, K., Matsuo, M., Niwa, J., 2001. Experimental study on parameters in localization of concrete subjected to compression. J. Materials, Conc. Struct., Pavements, JSCE 2001 (669):309–321. DOI: 10.2208/jscej.2001.669_309.

[14] Watanabe, K., Niwa, J., Yokota, H., & Iwanami, M., 2004. Experimental study on stress-strain curve of concrete considering localized failure in compression. Journal of Advanced Concrete Technology, 2(3): 395-407.

[15] Markeset, G., Hillerborg, A., 1995, Softening of concrete in compression – localization and size effects. Cement and Concrete Research, Vol. 24, No. 4, pp. 702-708, Elsevier Science Ltd.

[16] Shah, S.P., Choi, S., Jansen, D.C., 1994, Strain softening of concrete in compression. In: Proceedings of FraMCos 2, Zurich, Switzerland, pp. 1827-1841.